Optimal identification of Be-doped $Al_{0.29}Ga_{0.71}As$ Schottky diode parameters using Dragonfly Algorithm: a thermal effect study

Walid Filali[1*], **Rachid Amrani**[2,3], **Elyes Garoudja**[1], **Slimane Oussalah**[4], **Fouaz Lekoui**[5], **Zineb Oukerimi**[2], **Nouredine Sengouga**[6] and **Mohamed Henini**[7]

[1] *Plateforme Technologique de Microfabrication, Centre de Développement des Technologies Avancées, cité 20 août 1956, Baba Hassen, 16081 Alger, Algeria*
[2]*Département des Sciences de la Matière, Université Benyoucef Benkhedda Alger 1, Alger, Algeria*
[3]*LPCMME, Département de physique, Université d'Oran ES-Sénia, Oran, Algérie*
[4] *Division Microélectronique et Nanotechnologies, Centre de Développement des Technologies Avancées, cité 20 août 1956, Baba Hassen, 16081 Alger, Algeria*
[5] *Division Milieux Ionisés et Laser, Centre de Développement des Technologies Avancées, cité 20 août 1956, Baba Hassen, 16081 Alger, Algeria*
[6] *Laboratory of Metallic and Semiconducting Materials (LMSM), Université Mohamed Khider Biskra, BP 145 RP, 07000 Biskra, Algeria*
[7] *School of Physics and Astronomy, University of Nottingham, Nottingham, NG7 2RD, UK*

*Corresponding author email: wfilali@cdta.dz / walid.filali@live.fr

Abstract

In this work, a recent heuristic method called Dragonfly Algorithm (DA) has been employed for the first time to investigate the temperature effect on the Schottky diode electrical parameters. Beryllium-doped $Al_{0.29}Ga_{0.71}As$ Schottky diodes grown by molecular beam epitaxy (MBE) have been used to validate the suggested method. The proposed approach is based on the analysis of current-voltage-temperature (I-V-T) and capacitance-voltage (C-V) characteristics. Furthermore, the interface state density (N_{ss}) as function of the difference between the surface state energy and valence band energy ($E_{ss} - E_V$) was determined. The obtained results demonstrate the high efficiency of this strategy to accurately determine the electrical parameters and investigate their temperature dependency. This efficiency can be clearly remarked from the well fit between both predicted and measured current characteristics.

Keywords: AlGaAs/GaAs heterostructure; Dragonfly Algorithm; interface states; parameters identification; Schottky diode; temperature effect.

1. Introduction

Among III-V materials, AlGaAs/GaAs heterostructures have gained much importance. This is due to the variety of their applications in multitude fields and operation under several conditions (temperature, frequency, voltage) [1, 2]. That is why the elaboration mastery of such structures has a crucial role in the realization of essential smart electronic devices for the consumer electronics and optoelectronics market [3-5]. Metal-semiconductor (MS) structures are one of the most widely used rectifying contacts in electronics industry. Owing to the

performance and stability of those structures [6], these devices have been extensively investigated. However, up to now, a satisfactory understanding of all aspects has still not been reached. Ideality factor (n), barrier height (Φ_b), series resistance (R_s) and saturation current (I_s) are the main electronic parameters of Schottky barrier diodes (SBD) [7, 8]. Moreover, the SBD performance and reliability are significantly influenced by the presence of interface states (N_{ss}) between deposited metal and semiconductor surface [9, 10].

Several studies have been carried out to investigate the conduction phenomena and transport mechanisms in AlGaAs-based devices [1, 11]. Electrical characterization was considered as an indispensable phase, for instance current-voltage (I-V) and capacitance-voltage (C-V) characteristics were used to extract the main SBD parameters. However, I-V measurements of Schottky diodes at room temperature do not give sufficient information about the conduction mechanism and barrier formation nature at MS interface [12]. Thereby, many researchers have been interested in the investigation of temperature effects on I-V and C-V characteristics by determining the SBD parameters. In fact, several methods have been developed and are mainly classified into two categories, as analytical and optimization algorithms-based methods. [13-16]. Analytical approaches employ basic equations that deal with the Schottky diode conduction mechanism to identify their principle electronic parameters. Among the well-known analytical methods, the standard method is the most commonly used one to obtain both ideality factor and barrier height from I-V characteristics. In the presence of high series resistance which causes a narrowing in the linear region of I-V behavior, this approach loses its reliability [17]. To overcome this obstacle, Nord has suggested a new method that takes in consideration the influence of series resistance. However, its chief drawback is the unsuitability for the non-ideal Schottky contact, contrary to the abrupt contact metal/semiconductor assumption [18]. Bohlin method was then proposed to calculate Schottky diode parameters even with a non-ideal M/S contact [19]. In addition, another methodology to determine the SBD parameters from forward bias has been adopted by Cheung [13]. Additionally to what was previously mentioned, analytical methods require a critical choice of initial values for the unknown parameters and they depend on derivative and integrative functions. Also, each parameter is individually calculated based on I-V or C-V behaviors in a restricted region by neglecting the other parameters effect [20].

On the other hand, to overcome the previously cited shortcomings and since the SBD parameters identification is a multidimensional problem, optimization algorithms-based methods have been proposed [21]. These methods use optimization algorithms to identify the desired parameters based on an iterative mechanism, minimizing the gap between the measured and fitting curves. In literature, several authors have been interested in applying this category of methods. By utilizing Lambert W function, the thermionic emission equation was solved but it can converge to local optimum instead of global one [20, 21]. Also, heuristic-based optimization algorithms have been introduced to deal with the identification concern such as artificial bee colony (ABC) [22]. particle swarm optimization (PSO) [23], differential evolution (DE) [24] and Antlion optimizer (ALO) [25]. Each of these algorithms mimics specific behavior to solve an optimization problem. Those methods show a high efficiency and accuracy in optimizing a multi-model cost functions with ability to handle nonlinear functions with no need to derivative equations. Furthermore, the prior knowledge of the starting

conditions is not crucial in contrast with analytical methods [21]. SBD parameters extraction has been carried out using heuristic-based approaches by several researchers. A comparative study of several algorithms was done to identify a multi-quantum wells (MQW) AlGaAs Schottky diode from I-V-T characteristics [16]. The efficiency of the obtained results was evaluated by calculating several statistical test metrics. Another study for the estimation of SBD parameters using equilibrium optimizer (EO) has been elaborated [20]. A significant reliability and effectiveness was remarked from the obtained results. An efficient recent algorithm, called Dragonfly Algorithm (DA) [26] was employed to solve real world optimization problems [27]. DA proves a high efficiency and precision with a few tuning (control) parameters [21].

In this work, a new strategy based on DA was proposed to determine p-type AlGaAs/GaAs Schottky diode electrical parameters. n,Φ_b, R_s and I_s were extracted from I-V-T characteristics while effective density (N_{eff}) and built-in voltage (V_{bi}) were obtained from C-V measurements. Furthermore, the determination of interface state density as function of $(E_{SS} - E_V)$ was achieved. The significance of the obtained results was evaluated using statistical tests to prove the efficiency of the proposed strategy. The obtained results show a strong dependency of the previous mentioned parameters with temperature.

2. Experimental and characterization details

The Ti/Au/AlGaAs/GaAs/Au/Ni/Au Schottky diodes were fabricated using a semi-insulating GaAs substrate, with (100) crystal orientation. The AlGaAs/GaAs epitaxial layers were grown at a substrate temperature of 680 °C using a Varian Gen-II Molecular Beam Epitaxial (MBE) system. The layers consisted of an undoped GaAs buffer layer of 0.45µm thickness followed by the growth of 1µm Be-doped $Al_{0.29}Ga_{0.71}As$ layer (p-type doping = 10^{16} cm^{-3}). Then, metallization phase was carried out using EDWARDS E306 thermal evaporation system, in which the Schottky contacts were formed by the evaporation of Titanium (Ti) and Gold (Au) layers about 20 and 200 nm thicknesses, respectively. Finally, top layer has been etched to 600 nm in order to deposit ohmic contact Au/Ni/Au that was annealed at 360 °C [1]. The elaborated Schottky diodes were mounted on sample holder, which was located in helium closed cycle cryostat (Model Janis CCS-450) operating in the 10-450K temperature range. The I-V and C-V measurements were carried out using Keithley 428 and Boonton 7200, respectively.

3. Parameters determination strategy

3.1. Schottky diode model

For I-V measurements in an ideal Schottky diode, the current transport mechanism is due to thermionic emission (TE) and is given by [28]:

$$I = I_s\left(exp\left(\frac{q(V - IR_s)}{nkT}\right) - 1\right) \quad (1)$$

where I_s is the saturation current, and given by:

$$I_s = AA^*T^2 exp\left(\frac{-q\Phi_b}{kT}\right) \quad (2)$$

where n is the ideality factor, V is the applied bias voltage, q is the electron charge, k is the Boltzmann constant, R_s is the series resistance, T is the absolute temperature, Φ_b is the Schottky barrier height at zero bias, A* is the effective Richardson constant, and A is the area of the Schottky contact.

On the other hand, C-V characteristics of Schottky diode are expressed by [7]:

$$\frac{C}{A} = \sqrt{\frac{\pm q\varepsilon N_{eff}}{2(\pm V_{bi} \pm V - kT/q)}} \quad (3)$$

$$\frac{1}{(C/A)^2} = \frac{2\left(V_{bi} - V - \frac{kT}{q}\right)}{q\varepsilon N_{eff}} \quad (4)$$

where ε is the material permittivity, N_{eff} is the effective charge density in the depletion region and V_{bi} is the built-in voltage.

For p-type Schottky diode, which is the case of our elaborated samples, the "+" sign is applied in Eq. 3, and $N_{eff} \approx N_A$. This is due to the fact that $N_D \ll N_A$ [7].

3.2. Problem formulation

The main objective of this strategy is to extract Be-doped AlGaAs Schottky diode parameters, which lead to a minimum difference between both experimental and estimated characteristics. Mathematically, the identification process can be introduced as an optimization issue. The cost function to be minimized is defined as the Root Mean Square Error (RMSE) between measured and estimated characteristics. From I-V measurements, the value of $RMSE_{(I-V)}$ was computed using:

$$RMSE_{(I-V)} = \sqrt{\frac{1}{L}\sum_{i=1}^{L}[f_i(I_{mes}, V_{mes}, \eta)]^2} \quad (5)$$

where

$$f(I_{mes}, V_{mes}, \eta) = I_{mes} - \left(I_s\left\{exp\left[\frac{q(V_{mes} - I_{mes}R_S)}{nkT}\right] - 1\right\}\right) \quad (6)$$

On the other hand, $RMSE_{(C-V)}$ is given by:

$$RMSE_{(C-V)} = \sqrt{\frac{1}{S}\sum_{i=1}^{S}[g_i(C_{mes}, V_{mes}, \rho)]^2} \tag{7}$$

where

$$g(C_{mes}, V_{mes}, \rho) = C_{mes} - \left(A\sqrt{\frac{q\varepsilon N_A}{2(V_{bi} - V_{mes} - KT/q)}} \right) \tag{8}$$

I_{mes} and C_{mes} are measured current and capacitance, respectively. ρ and η are the vectors of parameters to be identified ($\eta = [n, \Phi_b, I_s, R_s]$ and $\rho = [N_{eff}, V_{bi}]$). L and S denote respectively the size of I-V and C-V curves (number of data points in I-V and C-V measurements).

The main goal of the strategy is to obtain the optimal values of the estimated parameters in such a manner that the RMSE will be the smallest as possible.

4. Dragonfly Algorithm

Dragonfly Algorithm (DA) is a recent population-based optimization algorithm developed by Mirjalili in 2016 [26]. The DA has demonstrated outstanding performance in a variety of continuous, discrete, single-objective, and multi-objective optimization problems. As real problem applications, DA has been employed by several researchers. In fact, a considerable variety of optimization problems in image processing, medical, robotic, physical science and engineering have been solved using DA [21].

It is mainly inspired from the hunting and migration strategies of dragonflies in nature. In this algorithm, hunting behavior of dragonflies is called static (feeding) swarm, while migration behavior is known as dynamic (migratory) swarm. Those behaviors are very close to the two essential stages of optimization when using other heuristic algorithms, such as exploration and exploitation. In static swarm, dragonflies form small clusters and fly in different areas to find food sources. In dynamic swarm, a huge number of dragonflies constitute one group and move along one direction. In DA, each dragonfly denotes a solution within the search space.

In order to guide the dragonflies to reach their paths, six weights are employed such as separation weight (s), alignment weight (a), cohesion weight (c), food factor (f), enemy factor (e), and the inertia weight (w). To ensure a best exploration of the search space, high alignment and low cohesion weights should be selected. However, to gain in exploitation, high cohesion and low alignment weights should be chosen. The balance between both exploration and exploitation can be established using an adaptive tuning of those weights.

In DA, five categories of behaviors are associated to the artificial dragonflies as depicted in Fig. 1, in the following manner:

- Separation: it is defined as the manner that dragonflies employ to ensure the separation from other agents. This behavior is mathematically modeled using Eq. (9).

$$S_i = -\sum_{j=1}^{N}(X - X_j) \tag{9}$$

where X is the current individual position, X_i is the position of the jth neighboring dragonfly, N represents the size of neighborhood.

- Alignment: it lies in determining how an agent can establish its velocity (speed) regarding the other adjacent dragonflies' velocity vectors. Alignment process is modeled using Eq. (10).

$$A_i = \frac{\sum_{j=1}^{N} V_j}{N} \tag{10}$$

where V_j is the jth neighbor velocity vector.

- Cohesion: it denotes the agents' tendency towards the herd center. Cohesion concept is given by Eq. (11).

$$C_i = \frac{\sum_{j=1}^{N} X_j}{N} - X \tag{11}$$

- Attraction: it denotes the attraction of agents to move towards food sources. The ith agent's tendency attraction to the food source is accomplished using Eq. (12):

$$F_i = X^+ - X \tag{12}$$

where $X^+$is the food source position.

- Distraction: it is defined as dragonfly proclivity to stay far away from predators. Distraction of the ith dragonfly and predator is given by Eq. (13).

$$E_i = X^- + X \tag{13}$$

where X^- is the predator position.

In this algorithm, the position vectors and food source fitness are updated using the best agent found so far, while those of enemies are updated according to the worst dragonfly. This consideration will allow DA to converge towards the most promising region of the search space and avoid non-promising areas.

In order to update dragonflies' positions, two vectors are used, such as step vector (ΔX) and position vector (X). The step vector defines the motion direction of dragonflies, and it is given according to Eq. (14).

$$\Delta_{X_{t+1}} = (sS_i + aA_i + cC_i + fF_i + eE_i) + wX_t \quad (14)$$

where: s, a, c, f and e denote the aforementioned weighting vectors.

Once the step vector computation is completed, the position vector will be computed based on Eq. (15).

$$X_{t+1} = X_t + \Delta_{X_{t+1}} \quad (15)$$

where t denotes the iteration.

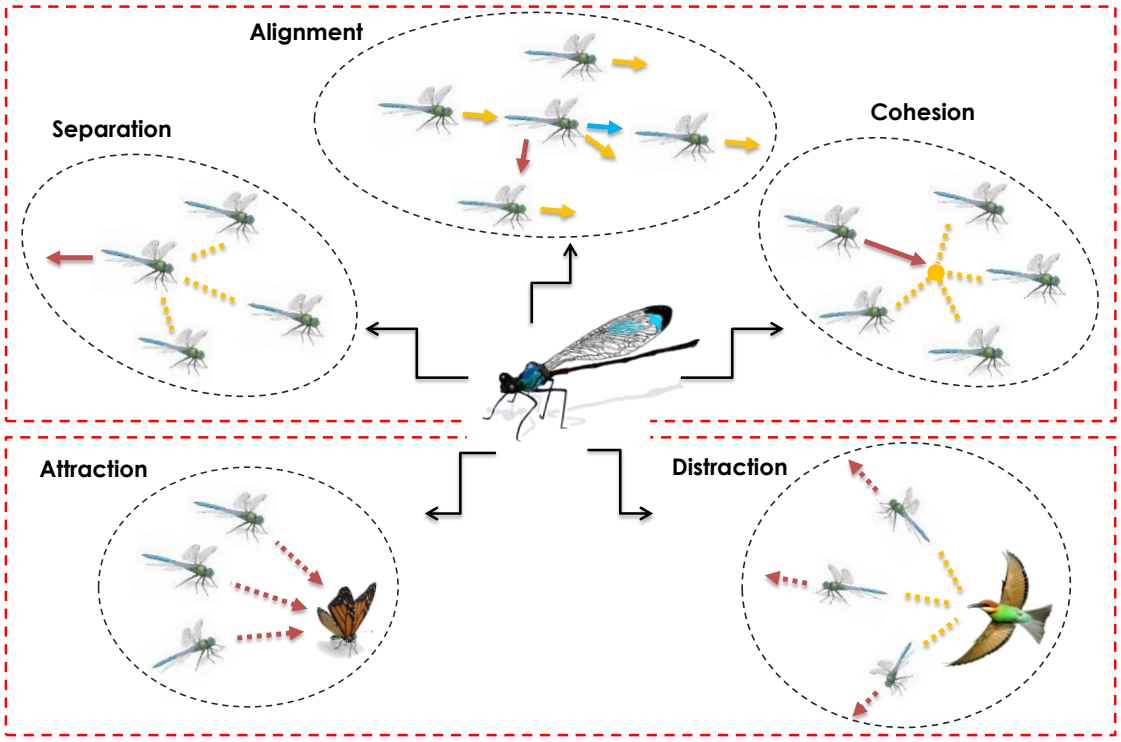

Fig. 1. Primitive corrective patterns between dragonflies.

The following is an explanation of DA's mathematical implementation. Consider an N-sized dragonfly population. The ith dragonfly's location is provided by:

$$X_i = \left(x_i^1, x_i^2, \ldots x_i^d, \ldots, x_i^N\right) \quad (16)$$

where N denotes the number of dragonflies agents in the swarm, i= 1, 2, 3 …, N. x_i^d is the *ith* dragonfly position in the *dth* search space dimension.

The fitness function is assessed on the basis the starting position values that are randomly produced according to the variable's lower and upper limits. After that, the six weights previously mentioned (s, a, c, f, e and w) are randomly initialized. The position and velocity vectors are updated after the calculation of separation, alignment and cohesion coefficients using Eqs. (9-11). Next, both attraction to the food sources and F_i and distraction from enemies E_i are computed using Eqs. (12-13). The neighborhood distance is computed using the Euclidean distance between the whole dragonflies and picking N of them. The Euclidean distance is given by:

$$r_{ij} = \sqrt{\sum_{k=1}^{d} \left(x_{i,k} - x_{j,k}\right)^2} \quad (17)$$

If there is at least one dragonfly in the vicinity, the dragonfly's velocity will be updated according to Eq. (14) and the dragonfly's location will be updated according to Eq. (15). If there is no dragonfly within the neighborhood radius, the dragonfly's position will be updated using the Levy Flight equation which is given by Eq. (18).

$$X_{t+1} = X_t + Levy(d)X_t \quad (18)$$

where more details about Levy Flight equation are cited in [29]. This fact will enhance both randomness and global search capacity of dragonflies. The cost (fitness) function is then assessed using the new position and velocity vectors. The procedure of the position update is iteratively repeated until the stop condition is satisfied. The stop criterion in this case is reaching the maximum number of cycles (MNC). Fig. 2 shows the DA algorithm flowchart.

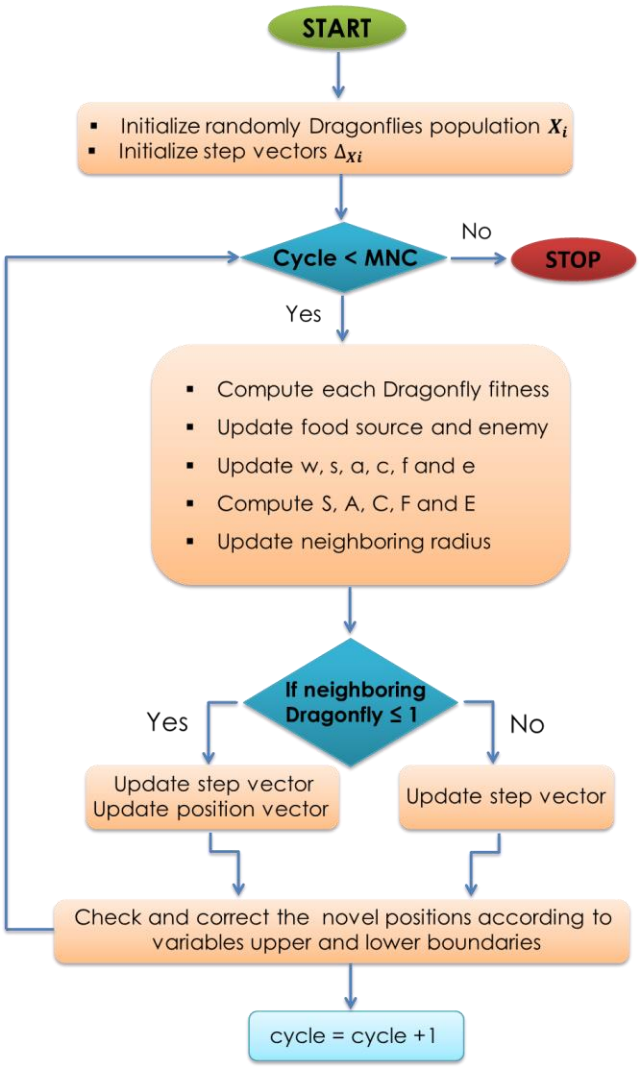

Fig. 2. Dragonfly Algorithm flowchart.

Dragonfly algorithm has several setting parameters, such as problem dimension (Dim), maximum number of iterations (MNC) and number of search agents. In this work those parameter are summarized in Table 1.

Table 1
DA algorithm setting parameters.

Setting parameters	I-V	C-V
Dim	3	2
MNC	500	500
Number of search agents	100	100

5. Results and discussion

Once the characterization stage was accomplished, the obtained data was treated using the proposed strategy. Fig. 3 shows the reverse and forward bias semi-log I-V characteristics of the elaborated Schottky diode at the temperature range 260-400 K. It can be seen a normal behavior of MS Schottky diodes, where it exhibits a rectifying comportment. The current increases exponentially with increasing both voltage and temperature, which is in good accordance with thermionic emission theory. The inset depicts the layer structure and the metal contacts of the elaborated devices, where the MS Schottky contact under study was made by Ti/Au.

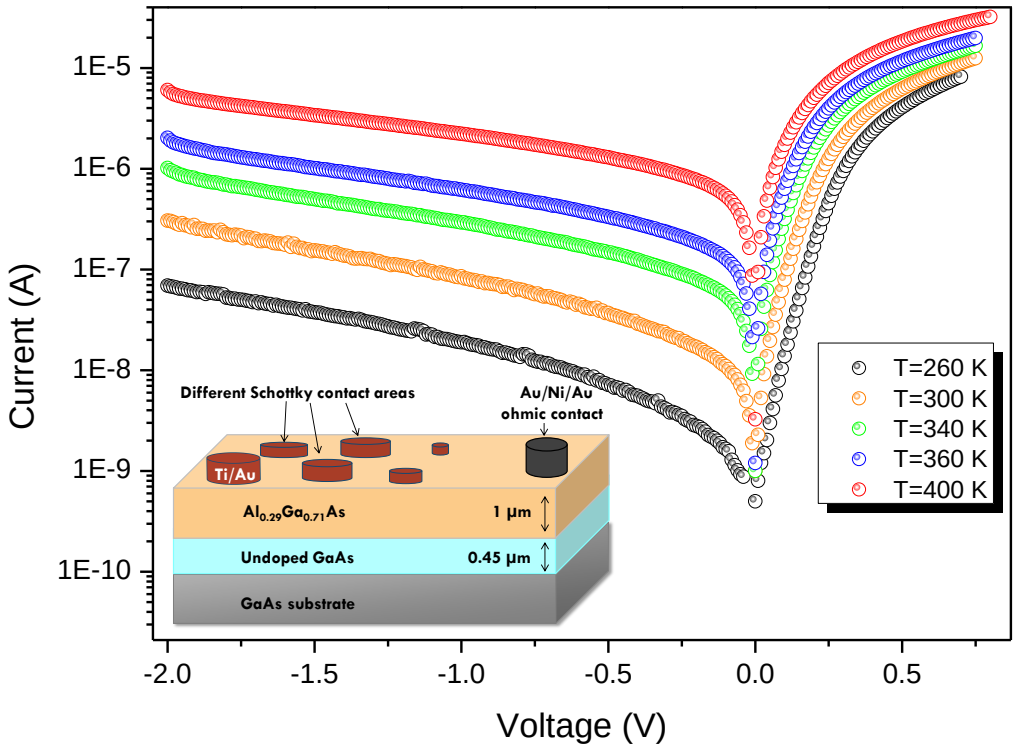

Fig. 3. Semi-log plot of I-V characteristics of p-type Ti-Au/AlGaAs/GaAs Schottky diode at different temperatures. Inset shows the schematic of the device structure.

Fig. 4 shows the $1/C^2$ -V plot for high frequency value (1 MHz) at room temperature. At high frequencies, the interface states cannot track the alternative-current (ac) signal of measurement, since carriers life time τ is highly greater than $1/2\pi f$ [9] Therefore, the effect of interface states is considered as negligible.

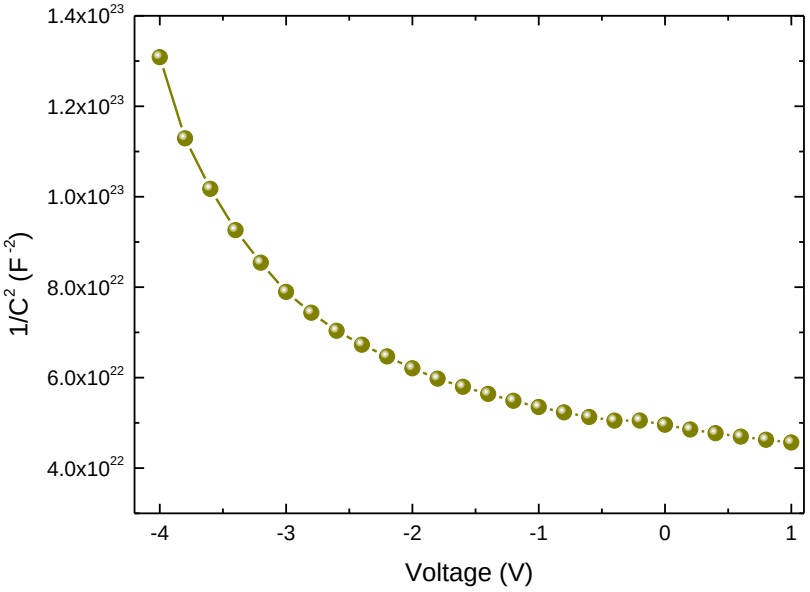

Fig. 4. Room temperature $1/C^2$ versus voltage plot for p-type Ti-Au/AlGaAs/GaAs Schottky diode at 1 MHz.

The estimated electrical parameters obtained after the optimization (minimization) stage are shown in Table 2, where a high thermal dependence of SBD parameters is observable. Another approach to present the accuracy of the identified parameters is suggested by plotting both experimental and DA-based estimated characteristics, as shown in Fig. 5. In fact, the parameters thus obtained are replaced in Eq.(1) to compute the estimated current. Fig. 5 shows a good fit between measured and estimated I-V curves even changing the temperature, which confirms the high capability of DA algorithm to accurately identify the diode electrical parameters.

By increasing the temperature, it is clearly seen in Fig. 6 that the ideality factor decreases and barrier height increases. Concerning n, the deviation from unity (ideal value of n is equal 1) indicates the presence of generation-recombination traps at the interface between the top of the structure and the Schottky contact. It is due also to the inhomogeneity of barrier height through the MS contact [20].

It is also noticed a proportional increase of Φ_b with temperature, which may be attributed to the variation of $Al_{0.29}Ga_{0.71}As$ band gap energy as function of temperature. Knowing that for a thermally activated process, the transport mechanism is expressed by the ability of charge carriers to cross the barrier. Another explanation of this behavior of Φ_b is the rise of quasi-Fermi level for the majority charge carriers to semiconductor side.

Fig. 7(a) shows an increase in R_s value with decreasing temperature. This behavior is due to the decrease of carrier mobility and lack of free carrier at low temperature values [30]. As seen in Fig. 7(b), the built-in voltage values increase with temperature. This effect is commonly due to the presence of traps in Ti-Au/AlGaAs interface [12].

Table. 2

SBD parameters identification results using DA algorithm from I-V and C-V characteristics.

T (K)	Schottky diode parameters					
	I-V				C-V	
	n	$\Phi_b\ (eV)$	$R_s\ (\Omega)$	I_s (A)	$N_{eff}(cm^{-3})$	$V_{bi}\ (eV)$
260	2.49	0.54	$39\ x10^{3}$	$9.2x10^{-9}$	$7.08x10^{14}$	-1.44
300	2.15	0.60	$33.8x10^{3}$	$3.42x10^{-8}$	$6.46x10^{14}$	-1.21
340	1.44	0.67	$30.9x10^{3}$	$5.68x10^{-8}$	$4.85x10^{14}$	-0.94
360	1.4	0.77	$29.5x10^{3}$	$1x10^{-8}$	$4.21x10^{14}$	-0.79
400	1.3	0.79	$20.3x10^{3}$	10^{-7}	$2.69x10^{14}$	-0.36

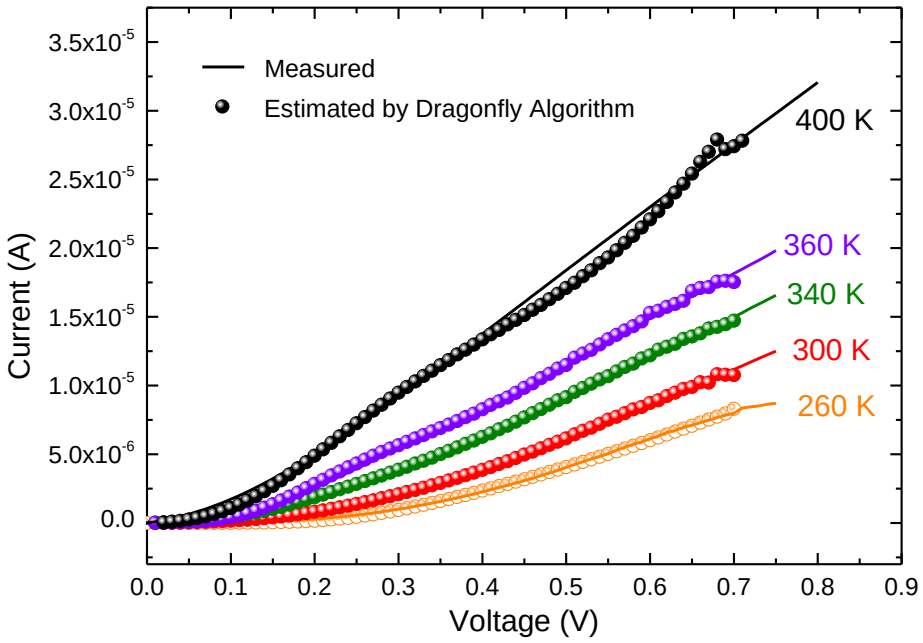

Fig. 5. Measured and estimated linear I-V characteristics for different temperatures.

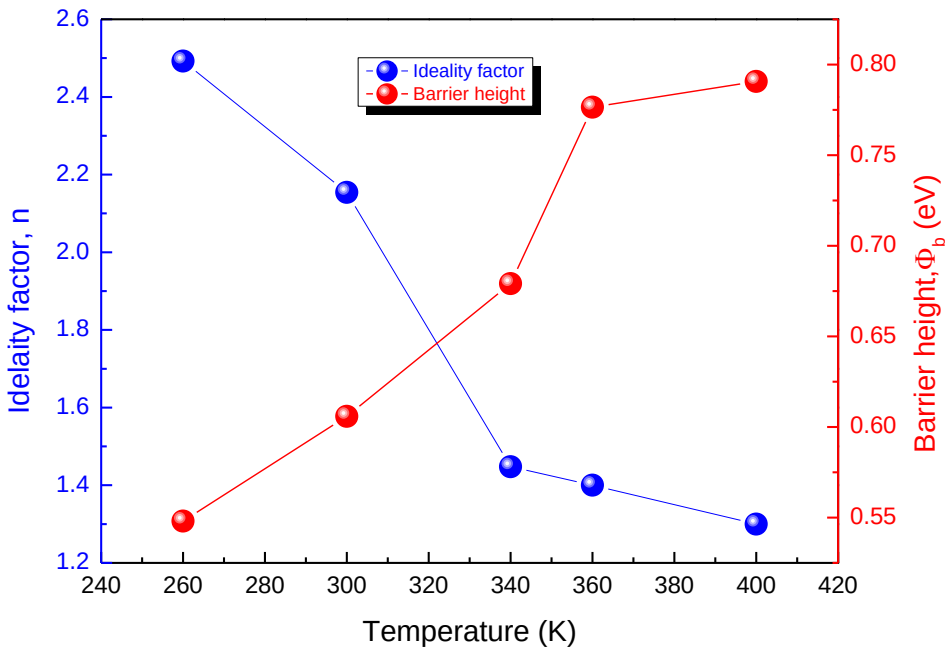

Fig. 6. Plots of the ideality factor and barrier height as a function of temperature for Ti/Au/ p-type AlGaAs/GaAs Schottky diodes.

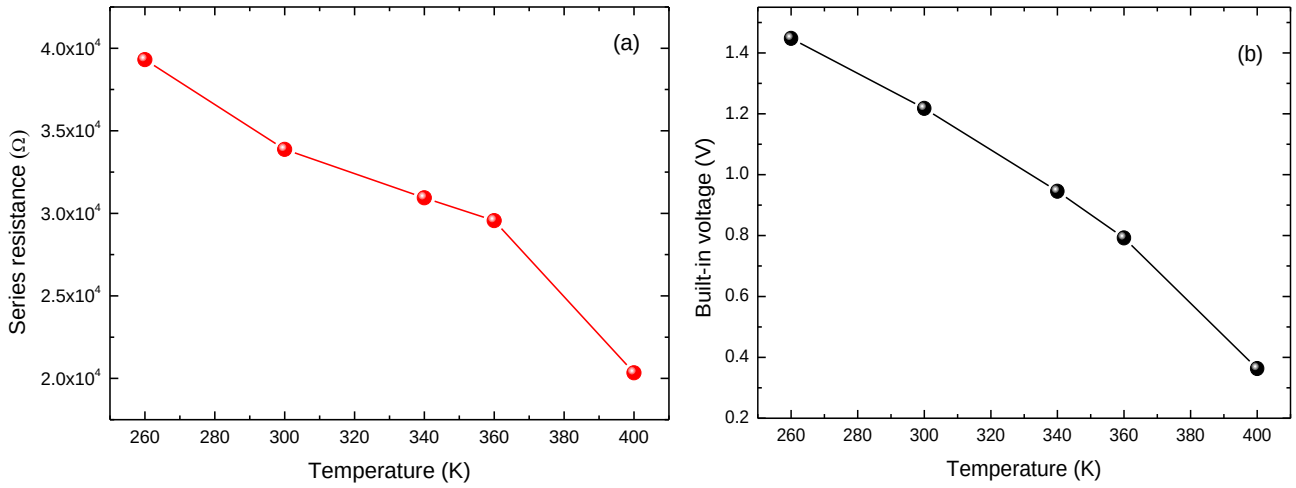

Fig. 7. Plots of temperature dependency of (a) series resistance and (b) built-in voltage of Ti/Au/ p-type AlGaAs/GaAs Schottky diodes.

Moreover, in order to test the accuracy of the determined parameters, four statistical evaluation criteria have been used such as Mean Square Error (MSE), Root Mean Square Error (RMSE), Mean Absolute Error (MAE) and R-squared (R^2). Those statistical metrics are computed as follows [31].

$$MSE = \frac{1}{L}\sum_{i=1}^{L}(y_i - \hat{y}_i)^2 \tag{19}$$

$$RMSE = \sqrt{\frac{1}{L}\sum_{i=1}^{L}(y_i - \hat{y}_i)^2} \tag{20}$$

$$MAE = \frac{1}{L}\sum_{i=1}^{L}|y_i - \hat{y}_i| \tag{21}$$

$$R^2 = 1 - \frac{\sum_{i=1}^{L}(y_i - \hat{y}_i)^2}{\sum_{i=1}^{L}(y_i - \bar{y})^2} \tag{22}$$

where y_i is the real measured current value, $\hat{y}_i$ is the corresponding estimated current value. L denotes the size of current vector (amount of samples). $\bar{y}$ is the mean value of current vectors. The obtained statistical metrics are summarized in Table 3.

Table 3
Statistical metrics evaluation results.

Metrics	260K	300K	340K	360K	400K
MSE	6.617×10^{-15}	1.618×10^{-14}	2.458×10^{-14}	5.232×10^{-14}	4.910×10^{-13}
RMSE	8.135×10^{-8}	1.272×10^{-7}	1.567×10^{-7}	2.287×10^{-7}	7.007×10^{-7}
MAE	6.852×10^{-8}	1.090×10^{-7}	1.356×10^{-7}	1.905×10^{-7}	5.558×10^{-7}
R^2	0.98	0.972	0.976	0.96	0.94

Results in Table 3 clearly demonstrate that the thermionic emission model with the identified parameters well fit the measured current-voltage characteristics for the different temperatures. This can be clearly observed from R^2 values that are higher than 0.9. Also, the low values of MSE, RMSE and MAE prove once again the high effectiveness of DA algorithm to accurately determine the SBD parameters.

Scatter plot between measured and predicted currents are depicted in Fig. 8.

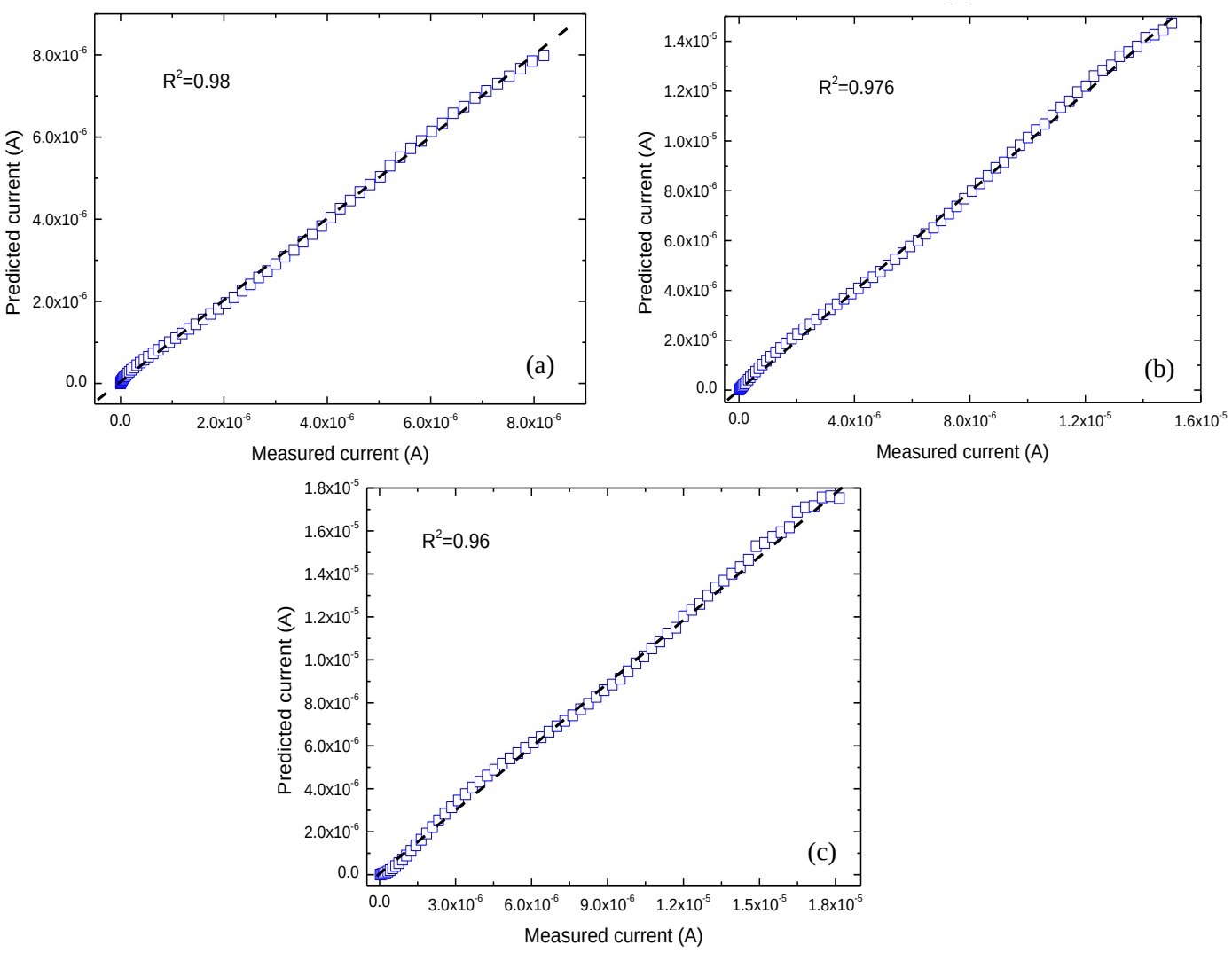

Fig. 8. Scatter plot between measured and predicted current for (a) 260K, (b) 340K and (c) 360 K

As can be seen from Fig. 8, a moderately strong and positive relationship between both predicted and measured current, which lead to produce a correlation coefficient close to 1.

After having determined SBD parameters, voltage-dependent ideality factor $n(V)$ can be calculated using Eq. (23) [9]:

$$n(V) = \frac{q\,V}{k\,T\,ln\,(I/I_S)} \tag{23}$$

where V and I are bias voltage and experimental current, respectively. The effective barrier height Φ_e, which is supposed to be influenced by bias voltage, can be expressed as follow [9]:

$$\Phi_e = \Phi_b + \left(1 - \frac{1}{n(V)}\right)V \tag{24}$$

Once the effective barrier height is computed, the energy of interface states E_{ss} as function of valence band energy E_V is given by [32]:

$$Ess - Ev = q\ (\Phi_e - V) \tag{25}$$

Interface state density expression is given by Card et al [32] as follows:

$$N_{ss} = \frac{1}{q}\left[\frac{\varepsilon_i}{\delta}\ (n(V) - 1) - \frac{\varepsilon_s}{W_D}\right] \tag{26}$$

where ε_0 is the vacuum permittivity, $\varepsilon_s = 10.09\varepsilon_0$, which is AlGaAs semiconductor permittivity, $\varepsilon_i = 4\ \varepsilon_0$ denotes the interfacial layer permittivity. The thickness of interfacial layer is given as $\delta = 30$ Å [8, 32, 33] and W_D is the space charge region (depletion region) width, which is found based on Eq. (27) [28] as 1.46 µm.

$$W_D = \sqrt{\frac{2\varepsilon_s}{q\ N_A}(V_{bi} - V)} \tag{27}$$

where N_A is the ionized acceptor concentration.

Results of interface states distribution from I-V characteristics of the realized sample at 300 K are depicted in Table 4.

Table. 4
The interface state density obtained from I-V characteristics at 300 K.

V (V)	n	Φe (eV)	$(Ess - Ev)\ (eV)$	$N_{ss}\ (eV^{-1}\ cm^{-2})$
0.19	2.0056	0.7743	0.5843	7.373 x10^{12}
0.22	2.0997	0.7943	0.5743	8.066 x10^{12}
0.25	2.2116	0.8160	0.5660	8.891 x10^{12}
0.28	2.3357	0.8392	0.5592	9.806 x10^{12}
0.31	2.4668	0.8634	0.5534	1.077 x10^{13}
0.34	2.6027	0.8884	0.5484	1.177 x10^{13}
0.37	2.7423	0.9141	0.5441	1.280 x10^{13}
0.4	2.8829	0.9403	0.5403	1.383 x10^{13}
0.43	3.0242	0.9669	0.5369	1.487 x10^{13}
0.46	3.1666	0.9938	0.5338	1.592 x10^{13}
0.49	3.3087	1.0210	0.5310	1.697 x10^{13}
0.52	3.4498	1.0483	0.5283	1.801 x10^{13}
0.55	3.5900	1.0759	0.5258	1.904 x10^{13}
0.58	3.7302	1.1036	0.5236	2.008 x10^{133}
0.61	3.8706	1.1315	0.5215	2.111 x10^{13}
0.64	4.0090	1.1594	0.5194	2.213 x10^{13}
0.67	4.1470	1.1875	0.5175	2.315 x10^{13}
0.7	4.2837	1.2156	0.5156	2.416 x10^{13}

Fig. 9 shows the interface state density values as function of $(Ess - Ev)$ for different temperatures. N_{ss} values decrease with increasing value of energy distribution from 0.40 to 0.65 eV as function of temperature. This temperature dependency can be attributed to an atomic rearrangement and restructuring at MS interface. Furthermore, N_{ss} decrease from the top of Ev towards midgap. This can be due to the barrier height inhomogeneity, as reported previously [32, 34-36].

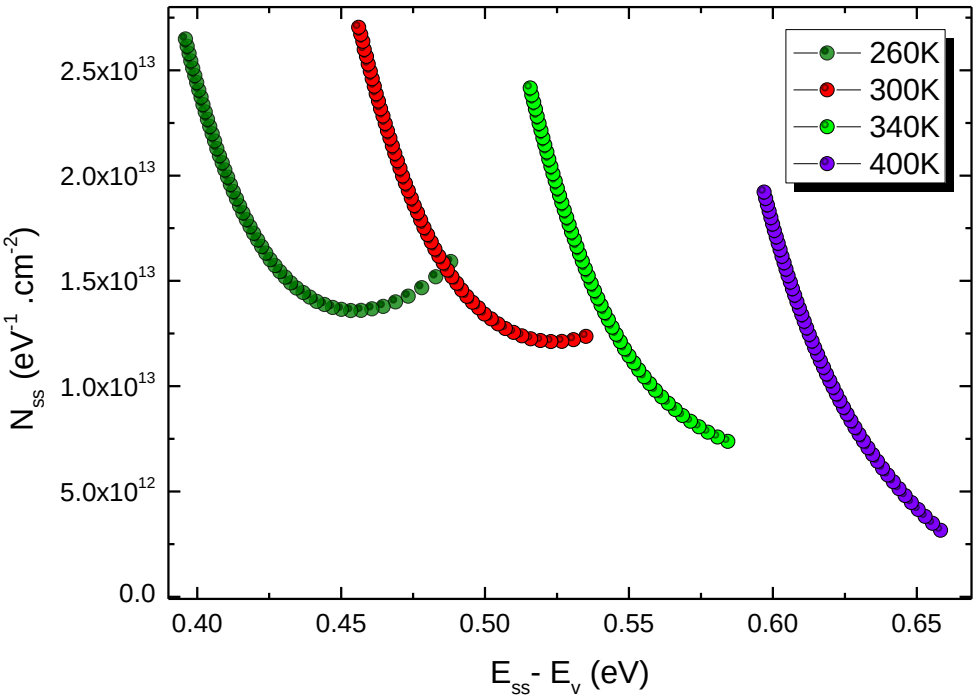

Fig. 9. Plot of interface states density distribution for Ti/Au/ p-type AlGaAs/GaAs Schottky diodes at different temperatures.

6. Conclusion

The thermal effect on the electrical properties of Be-doped AlGaAs/GaAs Schottky diodes has been investigated by I-V and C-V characteristics. The thermionic emission model of current mechanism has been used to determine the device electrical parameters using Dragonfly algorithm. The significance of the proposed method was judged by calculation of different statistical metrics. The low values of MSE, RMSE and MAE prove the high effectiveness of DA to accurately determine the SBD parameters. Furthermore, the closed to 1 of R-squared values indicate a good correlation between both measured and predicted current values. On the other hand, from I-V analysis, ideality factor values lie between 1.3 and 2.49 in the temperature range 260-400 K. Besides, the barrier height increased with temperature reaching a value of 0.79 eV. An apparent decrease in series resistance values with increasing temperature was observed, which is due to the rise of carriers' mobility. From C-V

characteristics, it was shown that when the temperature rises, the built-in voltage drops. The interface states are responsible for the low barrier height, which led to the higher-than-one obtained ideality factor. Nevertheless, even with the good obtained results, DA has low probability to trap in local optimum instead of global one. To deal with this issue, other variants of DA have been developed and will be employed in our future works.

References

[1] R.H. Mari, DLTS characterisation of defects in III-V compound semiconductors grown by MBE, in, University of Nottingham, 2011.

[2] R. Boumaraf, N. Sengouga, R. Mari, A. Meftah, M. Aziz, D. Jameel, N. Al Saqri, D. Taylor, M. Henini, Deep traps and temperature effects on the capacitance of p-type Si-doped GaAs Schottky diodes on (2 1 1) and (3 1 1) oriented GaAs substrates, Superlattices and Microstructures, 65 (2014) 319-331.

[3] J. Geisz, D. Friedman, III–N–V semiconductors for solar photovoltaic applications, Semiconductor Science and Technology, 17 (2002) 769.

[4] H.J. Joyce, Q. Gao, H.H. Tan, C. Jagadish, Y. Kim, J. Zou, L.M. Smith, H.E. Jackson, J.M. Yarrison-Rice, P. Parkinson, III–V semiconductor nanowires for optoelectronic device applications, Progress in Quantum Electronics, 35 (2011) 23-75.

[5] W. Filali, E. Garoudja, S. Oussalah, M. Mekheldi, N. Sengouga, M. Henini, A Novel Parameter Identification Approach for C–V–T Characteristics of Multi-Quantum Wells Schottky Diode Using Ant Lion Optimizer, Russian Microelectronics, 48 (2019) 428-434.

[6] A. TÜRÜT, On current-voltage and capacitance-voltage characteristics of metal-semiconductor contacts, Turkish Journal of Physics, 44 (2020) 302-347.

[7] D.K. Schroder, Semiconductor material and device characterization, John Wiley & Sons, 2015.

[8] H. Mathieu, H. Fanet, Physique des semiconducteurs et des composants électroniques, Dunod Paris, 2001.

[9] A. Tataroğlu, Ş. Altındal, Characterization of current–voltage (I–V) and capacitance–voltage–frequency (C–V–f) features of Al/SiO2/p-Si (MIS) Schottky diodes, Microelectronic engineering, 83 (2006) 582-588.

[10] J. Dhimmar, H. Desai, B. Modi, The effect of interface states density distribution and series resistance on electrical behaviour of Schottky diode, Materials Today: Proceedings, 3 (2016) 1658-1665.

[11] C. Sirtori, H. Page, C. Becker, V. Ortiz, GaAs-AlGaAs quantum cascade lasers: physics, technology, and prospects, IEEE journal of quantum electronics, 38 (2002) 547-558.

[12] W. Filali, N. Sengouga, S. Oussalah, R.H. Mari, D. Jameel, N.A. Al Saqri, M. Aziz, D. Taylor, M. Henini, Characterisation of temperature dependent parameters of multi-quantum well (MQW) Ti/Au/n-AlGaAs/n-GaAs/n-AlGaAs Schottky diodes, Superlattices and Microstructures, 111 (2017) 1010-1021.

[13] S. Cheung, N. Cheung, Extraction of Schottky diode parameters from forward current-voltage characteristics, Applied Physics Letters, 49 (1986) 85-87.

[14] Y. Chang, W. Mao, Y. Hao, A new parameter extraction method for Schottky barrier diodes, Chinese Journal of Electronics, 28 (2019) 497-502.

[15] W. Hao, C. Xing, X. Guang-Hui, H. Ka-Ma, A novel physical parameter extraction approach for Schottky diodes, Chinese Physics B, 24 (2015) 077305.

[16] E. Garoudja, W. Filali, S. Oussalah, N. Sengouga, M. Henini, Comparative study of various methods for extraction of multi-quantum wells Schottky diode parameters, Journal of Semiconductors, 41 (2020) 102401.

[17] J. Osvald, E. Dobrocka, Generalized approach to the parameter extraction from I-V characteristics of Schottky diodes, Semiconductor science and technology, 11 (1996) 1198.

[18] H. Norde, A modified forward I-V plot for Schottky diodes with high series resistance, Journal of applied physics, 50 (1979) 5052-5053.

[19] K. Bohlin, Generalized Norde plot including determination of the ideality factor, Journal of applied physics, 60 (1986) 1223-1224.

[20] A. Rabehi, B. Nail, H. Helal, A. Douara, A. Ziane, M. Amrani, B. Akkal, Z. Benamara, Optimal estimation of Schottky diode parameters using a novel optimization algorithm: Equilibrium optimizer, Superlattices and Microstructures, 146 (2020) 106665.

[21] Y. Meraihi, A. Ramdane-Cherif, D. Acheli, M. Mahseur, Dragonfly algorithm: a comprehensive review and applications, Neural Computing and Applications, (2020) 1-22.

[22] D. Karaboga, B. Basturk, A powerful and efficient algorithm for numerical function optimization: artificial bee colony (ABC) algorithm, Journal of global optimization, 39 (2007) 459-471.

[23] Y. Jiang, T. Hu, C. Huang, X. Wu, An improved particle swarm optimization algorithm, Applied Mathematics and Computation, 193 (2007) 231-239.

[24] A.K. Qin, V.L. Huang, P.N. Suganthan, Differential evolution algorithm with strategy adaptation for global numerical optimization, IEEE transactions on Evolutionary Computation, 13 (2008) 398-417.

[25] S. Mirjalili, The ant lion optimizer, Advances in engineering software, 83 (2015) 80-98.

[26] S. Mirjalili, Dragonfly algorithm: a new meta-heuristic optimization technique for solving single-objective, discrete, and multi-objective problems, Neural Computing and Applications, 27 (2016) 1053-1073.

[27] M. Alshinwan, L. Abualigah, M. Shehab, M. Abd Elaziz, A.M. Khasawneh, H. Alabool, H. Al Hamad, Dragonfly algorithm: a comprehensive survey of its results, variants, and applications, Multimedia Tools and Applications, (2021) 1-38.

[28] E.H. Rhoderick, R.H. Williams, Metal-semiconductor contacts, Clarendon Press, 1988.

[29] X.-S. Yang, Firefly algorithm, Levy flights and global optimization, in: Research and development in intelligent systems XXVI, Springer, 2010, pp. 209-218.

[30] Ş. Karataş, Ş. Altındal, A. Türüt, M. Çakar, Electrical transport characteristics of Sn/p-Si schottky contacts revealed from I–V–T and C–V–T measurements, Physica B: Condensed Matter, 392 (2007) 43-50.

[31] D. Chicco, M.J. Warrens, G. Jurman, The coefficient of determination R-squared is more informative than SMAPE, MAE, MAPE, MSE and RMSE in regression analysis evaluation, PeerJ Computer Science, 7 (2021) e623.

[32] H. Card, E. Rhoderick, Studies of tunnel MOS diodes I. Interface effects in silicon Schottky diodes, Journal of Physics D: Applied Physics, 4 (1971) 1589.

[33] A. Cowley, S. Sze, Surface states and barrier height of metal-semiconductor systems, Journal of applied physics, 36 (1965) 3212-3220.

[34] V. Janardhanam, I. Jyothi, P.S. Reddy, J. Cho, J.-M. Cho, C.-J. Choi, S.-N. Lee, V.R. Reddy, Double Gaussian barrier distribution of permalloy (Ni0. 8Fe0. 2) Schottky contacts to n-type GaN, Superlattices and Microstructures, 120 (2018) 508-516.

[35] R. Tung, Electron transport at metal-semiconductor interfaces: General theory, Physical Review B, 45 (1992) 13509.

[36] I. Jyothi, M.-W. Seo, V. Janardhanam, K.-H. Shim, Y.-B. Lee, K.-S. Ahn, C.-J. Choi, Temperature-dependent current–voltage characteristics of Er-silicide Schottky contacts to strained Si-on-insulator, Journal of alloys and compounds, 556 (2013) 252-258.